JGR Planets

RESEARCH ARTICLE
10.1029/2022JE007721

Can Archean Impact Structures Be Discovered? A Case Study From Earth's Largest, Most Deeply Eroded Impact Structure

M. S. Huber[1], E. Kovaleva[1,2], A. S. P. Rae[3], N. Tisato[4,5], and S. P. S. Gulick[4,5,6]

[1]Department of Earth Science, University of the Western Cape, Bellville, South Africa, [2]Helmholtz Centre Potsdam, GFZ, Potsdam, Germany, [3]Department of Earth Sciences, University of Cambridge, Cambridge, UK, [4]Department of Geological Sciences, Jackson School of Geoscience, University of Texas at Austin, Austin, TX, USA, [5]Center for Planetary Systems Habitability, University of Texas at Austin, Austin, TX, USA, [6]Institute for Geophysics, Jackson School of Geoscience, University of Texas at Austin, Austin, TX, USA

Abstract The record of terrestrial impact events is incomplete with no Archean impact structures discovered, despite the expected abundance of collisions that must have occurred. Because no Archean impact structures have been identified, the necessary conditions to preserve an impact structure longer than 2 Byr are unknown. One significant effect of shock metamorphism is that the physical properties of the target rocks change, resulting in distinctive geophysical signatures of impact structures. To evaluate the preservation potential of impact structures, we evaluate the deeply eroded Proterozoic Vredefort impact structure to examine the changes in physical properties and the remnant of the geophysical signature and compare the results with the well-preserved Chicxulub impact structure. The major structural features of Vredefort are similar to the expected profile of the Chicxulub structure at a depth of 8–10 km. The Vredefort target rocks, while shocked, do not preserve measurable changes in their physical properties. The gravity signature of the impact structure is minor and is controlled by the remnant of the collapsed transient crater rim and the uplifted Moho surface. We anticipate that erosion of the Vredefort structure by an additional 1 km would remove evidence of impact, and regardless of initial size, erosion by >10 km would result in the removal of most of the evidence for any impact structure from the geological record. This study demonstrates that the identification of geologically old (i.e., Archean) impact structures is limited by a lack of geophysical signatures associated with deeply eroded craters.

Plain Language Summary Meteorite collisions should have formed throughout the 4.5 billion-year-long history of Earth, but we have only found impact craters that are less than half of the age of the Earth (2 billion years) and younger. In order to understand how to find very old impact craters, we studied the largest of the oldest preserved impact craters. The 2 Byr old Vredefort structure in South Africa has been deeply eroded, and thus provides a good view of its deep roots. We collected a series of samples of the exposed rocks known to have evidence of shock effects and measured their physical properties. We found that the physical properties do not show evidence of the meteorite impact event. We also established that the gravity profile of the crater preserves a weak signal. When the Vredefort structure erodes a bit more, the geophysical characteristics that make it identifiable will be gone. We expect that signatures of ancient impact structures even larger than Vredefort would be completely removed by erosion by now. Therefore, to find very old impact craters, we need to look in areas that have experienced unusually little erosion.

Key Points:

- The target rocks exposed on the surface of the central core of the Vredefort structure do not preserve changes in physical properties
- Regardless of initial size, changes in the physical properties of impact structures on Earth might be unidentifiable if they are eroded by more than 10 km
- Archean impact structures on Earth can only be identified if extraordinary preservation takes place

Supporting Information:

Supporting Information may be found in the online version of this article.

Correspondence to:

M. S. Huber,
mhuber@uwc.ac.za

Citation:

Huber, M. S., Kovaleva, E., Rae, A. S. P., Tisato, N., & Gulick, S. P. S. (2023). Can Archean impact structures be discovered? A case study from Earth's largest, most deeply eroded impact structure. *Journal of Geophysical Research: Planets*, *128*, e2022JE007721. https://doi.org/10.1029/2022JE007721

Received 21 DEC 2022
Accepted 24 MAY 2023

1. Introduction

Hypervelocity impact craters are common features of the surfaces of rocky bodies within the solar system, with impact events occurring since the formation of the solar system (Taylor, 1992). The 4.5 Ga history of impacts is recorded on the Moon, but planets such as Earth and Venus have active surface processes that obliterate the evidence of older impact events. The record of impact events on Earth is known to be incomplete due to constant re-surfacing processes.

In total, only 18 of the ca. 200 known impact structures on Earth are confirmed to have formed in the Proterozoic (Schmieder & Kring, 2020), and none in the Archean. Evidence of impact events in the Archean is limited to 17 impact ejecta layers, with the oldest being 3.47 Ga (Byerly et al., 2002). In order to have a more complete record of impact cratering on Earth, Archean impact structures need to be discovered, but preserved Archean crust is

often deeply eroded and/or tectonically deformed. Thus, we need to study such properties of the oldest known impact structures to help facilitate the identification of new Archean and Paleoproterozoic structures.

The major effect of hypervelocity impacts on target rocks is changes in their physical properties, such as lowered density, increased porosity, and increased or decreased *P*- and *S*-wave velocity (Christeson et al., 2018; Pilkington & Grieve, 1992; Rae et al., 2019a, 2019b). Changes in physical properties through impact cratering have been linked to the overall high porosity of the lunar surface (Wiggins et al., 2022). Altering physical properties create gravity anomalies, which increase in diameter and magnitude as the size of the impact structure increases. It is also expected that the maximum magnitude of a gravity anomaly is achieved once the crater exceeds a particular diameter (depending on the planetary body), and impact structures above this diameter only have larger diameter gravity anomalies without larger magnitude (Pilkington & Grieve, 1992). Modeling results suggest that the change in physical properties on Earth caused by large impact events should only extend to a maximum depth of ca. 10 km (Pilkington & Grieve, 1992; Wiggins et al., 2022). If this is the case, no observable impact-related changes in the physical properties of the rocks below this depth will be observed, resulting in a disconnect between the measurable physical properties of target rocks and the remaining geophysical signature.

In order for an impact structure to be discovered, an anomaly related to the impact must be observable and definitive evidence of the impact must be preserved (Hergarten & Kenkmann, 2015). In this study, the deeply eroded Vredefort impact structure is tested for the detectable impact effects that can survive within the geological record. We collected samples along a transect through the core of the structure and measured the geophysical characteristics of each sample. We examined our results relative to expected values for rocks with similar petrology and to hydrocode impact modeling results. We then evaluated the degree to which the records of older impact structures can survive through time and determined that the erosional level of Vredefort is near the maximum erosional level at which evidence of impact could be detected.

2. Geological Setting

The Vredefort impact event occurred 2019 ± 2 Ma (Moser, 1997) within the Kaapvaal Craton, resulting in an impact structure that had an original diameter of at least 170 km based on numerical modeling (Ivanov, 2005) and had structural effects to a diameter of ca. 300 km (Friese et al., 1995). The center of the impact structure is located approximately 100 km SW of Johannesburg, South Africa, and is generally considered to coincide with the position of Lake Inlandsee (e.g., Hart et al., 2000). The target rocks included basement granites and granitoids (Tonalite-Trondhjemite-Granodiorite [TTG]) of the Kaapvaal craton, overlain by Dominion Group lavas, the Witwatersrand Supergroup, the Ventersdorp Supergroup, and the Transvaal Supergroup (Bisschoff, 1972). At 2.06 Ga, prior to the Vredefort impact event, the large layered mafic intrusion Bushveld Complex formed to the north-east (Cawthorn & Walraven, 1998), and intrusive dikes from the Bushveld event extended into the target area of Vredefort (Flowers et al., 2003).

After the impact event, the structure was subjected to extensive erosion, estimated to be between 7 and 10 km based on fluid inclusions (Schreyer, 1983), and between 8 and 11 km based on metamorphic *P-T* paths (Gibson et al., 1998). The erosion removed most impactites, including the melt sheet and proximal ejecta, as well as crater morphology including any form of crater rim or peak ring structure that may have existed. Thus, a deep profile through the impact structure is now exposed. The only remnants of impact melt rock are several impact melt dikes known as the "Vredefort Granophyre Dikes" (Koeberl et al., 1996). The impact structure was buried after the impact and then partially exhumed ca. 1 Ga later (Kovaleva et al., 2019), and then affected by Permian glaciation (Cavosie et al., 2017). More recently, the rocks of the Karoo supergroup buried the structure, and Jurassic dolerite dikes cut through some portions of the crater. The southeastern part of the impact structure is still covered by the Karoo Supergroup (Figure 1).

Presently, the primary exposure of the impact structure is within the Vredefort Dome, which has a "core" of granitoid and mafic crystalline rocks in the interior and a "collar" of metasedimentary and metavolcanic rocks (Bisschoff, 1972). This structure represents the formerly buried central uplift of the impact basin (Figure 1). The Vredefort Dome is surrounded by the Potchefstroom Synclinorium. The fold axis of the synclinorium is approximately 70–75 km radial distance from the center of the impact structure and follows the curvature of the collar rocks (Friese et al., 1995). Beyond the Potchefstroom Synclinorium, the Rand Anticline Thrust Zone is located at a radial distance of ca. 115 km from the center of the impact structure (Durrheim et al., 1991).

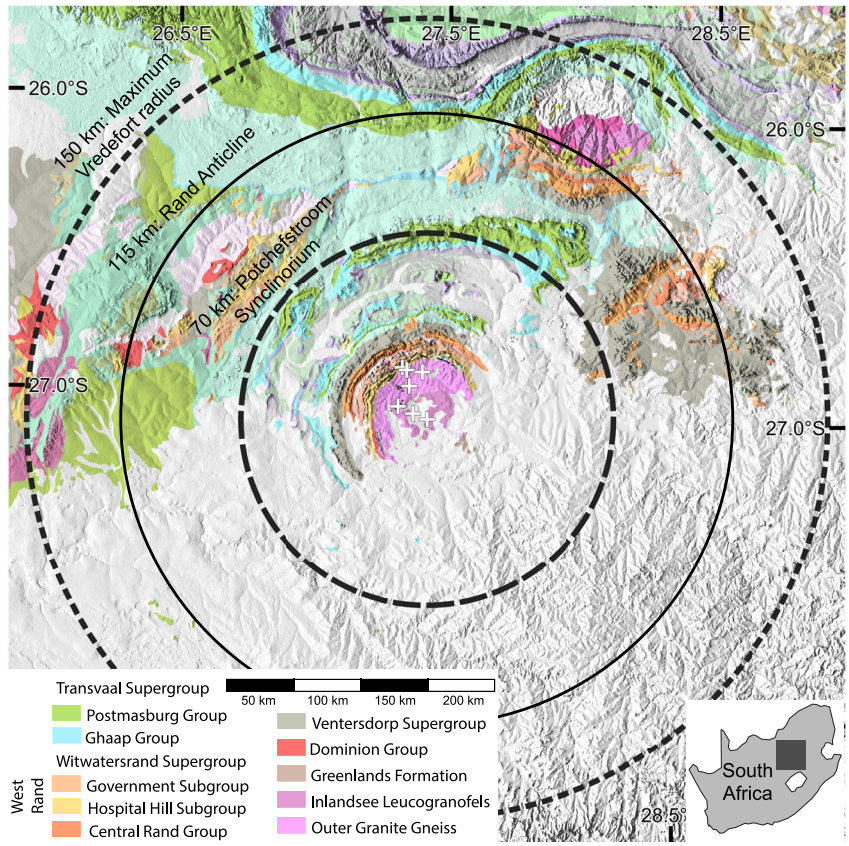

Figure 1. Geological map of the Vredefort impact structure overlain on a digital elevation model. Only Proterozoic and older geology are shown. The position of the Potchefstroom Synclinorium is plotted along with the maximum-estimated diameter of the impact structure. Sampling locations in this study are plotted as "+" symbols. Note that some symbols overlap due to their close proximity. Geological data from the South African Council for Geoscience. Terrane topography from the Shuttle Radar Topography Mission (Farr & Kobrick, 2000).

3. Materials and Methods

3.1. Samples

A profile of 11 samples were taken from the crystalline basement rocks of the Vredefort Dome for the purpose of measuring their geophysical characteristics (Figure 1, Table 1). The profile started from the Inlandsee, which, for the purpose of this study, is assumed to represent the center of the impact structure, and extended outwards to the boundary with the collar rocks along a non-linear profile. Samples were taken based on the availability of outcrops and access to property.

3.2. Petrography

Thin sections of each sample were prepared and analyzed petrographically to determine the precise rock types, degree of alteration of the samples, degree of shock effect, and visible extent of fracturing within the samples. Each thin section was point counted with a 2 × 2 mm grid to determine the mineralogical composition, resulting in approximately 200 points per thin section.

3.3. Geophysical Properties

The bulk rock properties were determined from 25 by 50 mm cores taken from the collected samples. The ultrasonic velocity (V_p and V_s) and porosity were measured at the Core Laboratories Inc., Houston, TX, USA, by the pulse-transmission method and the Boyle's Law method, respectively. For a broader comparison of the samples

Table 1
Samples With Results of Physical Property Measurements

Sample	Latitude (°)	Longitude (°)	Distance to crater center (km)	Bouger gravity (mGal)	Porosity (%)	Density (g/cm^3)	Compressional velocity (km/s)	Shear velocity (km/s)	Bulk modulus (PSI)	Young's modulus (PSI)	Shear modulus	Poisson's ratio	Composition
IS	−27.05243	27.48782	0	−115	0.96	2.601	5.170	3.179	4.94	9.01	3.77	0.196	Recrystallized granite
FNN-1	−27.03555	27.43327	5.7	−121	0.23	2.606	5.727	3.245	7.03	9.97	3.95	0.264	Recrystallized tonalite
HG-2	−27.01376	27.37654	11.8	−128	0.24	2.661	6.090	3.593	7.63	12.22	4.96	0.233	Vredefort Granophyre (impact melt)
HG-1	−27.01346	27.3763	11.9	−128	0.38	2.635	6.018	3.570	7.30	11.89	4.84	0.228	Granite
AWB-2	−26.94372	27.41463	14.1	−125	0.75	2.603	5.426	3.144	6.05	9.18	3.68	0.247	Granite with melt veins
AWB-1	−26.94439	27.41382	14.1	−125	1.19	2.783	5.315	3.167	5.88	9.72	3.97	0.225	Charnockite
PGE	−26.89433	27.46107	17.8	−131	0.57	2.623	5.200	3.263	4.85	9.45	4.02	0.175	Tonalite
SQ-2	−26.89006	27.40191	20.0	−113	0.87	2.621	5.233	3.139	5.38	9.07	3.72	0.219	Granite
SQ-1	−26.89004	27.40187	20.0	−113	0.23	2.620	5.184	3.371	4.39	9.66	4.26	0.133	Granite
KJK-1	−26.88219	27.38531	21.4	−102	1.20	2.660	5.309	3.251	5.33	9.59	4.00	0.200	Granite
KJK-2	−26.88217	27.38528	21.5	−102	0.69	2.644	5.550	3.318	6.09	10.16	4.16	0.222	Foliated metagranite

with the larger structure, the Bouguer gravity data of the Vredefort structure and surrounding area, provided by the South African Council for Geoscience, were analyzed using QGIS 3.22.

3.4. Rock Physics Modeling

Using Matlab, we calculated the theoretical densities and elastic properties of each sample using effective medium theories and the mineral abundances (f_i) that were obtained by the point counting. For each mineral, we used two extreme values of density, bulk, and shear modulus assuming that plagioclase is a solid solution of anorthite-albite, K-feldspar is microcline, biotite is muscovite or chlorite, serpentine could be either chrysotile or antigorite, clinopyroxene is a solid solution of enstatite-ferrosilite, and opaque minerals are solid solutions of magnetite-rutile. Maximum and minimum values for each possible bulk (K) and shear (G) modulus for mineral assemblage were determined. Finally, for each rock sample, we calculated *P*- and *S*-wave velocities for the Voigt (VpV and VsV) and the Voigt-Reuss-Hill (VpVRH and VsVRH) bounds. Values for literature data were also calculated using the same script. Reference samples of Aue granite (AUE, Stanchits et al., 2006), Westerly granite (WSG, Brace, 1965; Coyner, 1984; Krech & Chamberlain, 1974; Siegfried & Simmons, 1978), Chelmsford granite (CHF, Coyner, 1984; Todd, 1973), Barre granite (BRR, Birch, 1960; Coyner, 1984; Krech & Chamberlain, 1974), and Chicxulub granite (CHX, Morgan et al., 2017) were used. See Supporting Information S1 for details on the precise calculations made.

3.5. Hydrocode Modeling

A numerical simulation of the Vredefort impact event was performed to provide a comparison between the observed and modeled physical properties of the samples from the structure. Here, we used the parameters presented by Ivanov (2005) for the Vredefort event using the iSALE-2D shock physics code (Wünnemann et al., 2006). iSALE is based on the SALE hydrocode solution algorithm (Amsden et al., 1980) modified to include an elasto-plastic constitutive model, fragmentation models, various equations of state, and multiple materials (Ivanov et al., 1997; Melosh et al., 1992). In the early 2000's, a modified strength model was developed (Collins et al., 2004), resulting in the versatile shock physics code, SALEB, capable of simulating impact events from the first contact of the impactor with the target to the cessation of the gravity-driven collapse of the crater. This code was presented and used by Ivanov (2005) to model the Vredefort impact event. The SALEB code was subsequently developed into iSALE with improvements including a porosity compaction model (Collins et al., 2011; Wünnemann et al., 2006), and a dilatancy model (Collins, 2014).

In summary, the impact event is simulated with a 14-km diameter projectile at an impact velocity of 15 km/s. The target is composed of three layers: an upper layer, 14 km thick, of metamorphosed sediments with an equation of state for quartzite (Melosh, 2007); a middle layer, 31 km thick, of crust with an equation of state for granite (Pierazzo et al., 1997); and a lower layer representing the mantle with an equation of state for dunite (Benz et al., 1989). The geothermal gradient through the lithosphere was defined as 17.5 K/km. For further details, see Ivanov (2005). The only modification that we added to the parameters of Ivanov (2005) is the inclusion of dilatancy (Collins, 2014), which quantifies the volume change, that is, pore opening/closure, that occurs while the rocks undergo shear deformation. We used the recommended low-Geological Strength Index (GSI) dilatancy parameters for all lithologies (see Collins (2014), for further details). The input files of our simulation are included in Supporting Information S1.

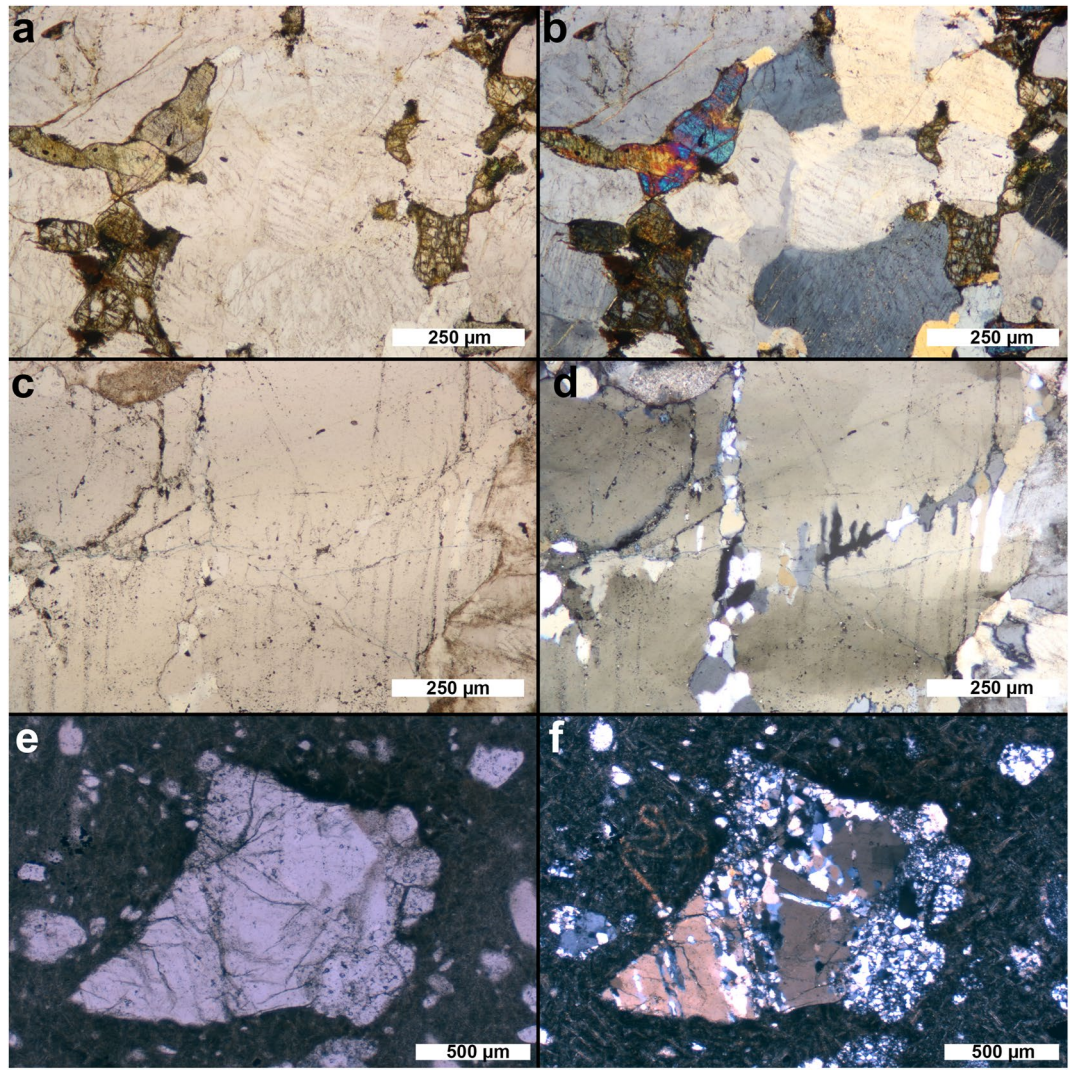

Figure 2. Petrography of samples in this study. (a). Charnockite sample AWB-1. This sample was measured to have high porosity with a midrange velocity. Plane-polarized light (PPL). (b). Same area as in panel (a), cross-polarized light (XPL). (c). Quartz grain from sample PGE with shock features that have been recrystallized. PPL. (d). The same area as in panel (c), XPL. (e). Impact melt from sample HG-2 with partially recrystallized quartz inclusion, PPL. (f). The same area as in panel (e), XPL.

4. Results

4.1. Samples and Petrography

Using the Inlandsee as the central point of the impact structure, samples were taken at radial distances between 0 and 21.5 km from the center (Table 1). Two samples are the impact melt rocks (HG-2 and FNN-2). Of the remaining crystalline rocks, based on the modal analysis of thin sections, six are granites (Figures 2a and 2b), two are granodiorites (FNN-1 and IS-1), one is a charnockite (AWB-1), and one is a quartz-rich granitoid (AWB-1). The granites and granitoids have experienced low-grade metamorphism, and bear evidence of recrystallization and metasomatic reactions. Myrmekitic textures are common in the granites and granitoids (Figures 2a and 2b). Sericite after plagioclase and chlorite after biotite alterations are prevalent in many of the samples (Figure 2), and sample SQ-2 contains epidote. Remnants of shock effects are present in all of the samples, particularly expressed as recrystallized planar deformation features and planar fractures in quartz. Two of the samples have mm-wide pseudotachylite veins transecting the thin sections (Figures 2e and 2f; KJK-1, and AWB-2), so that 1–2 area % of the thin sections are composed of pseudotachylitic material. The impact melt rock HG-2 has a typical

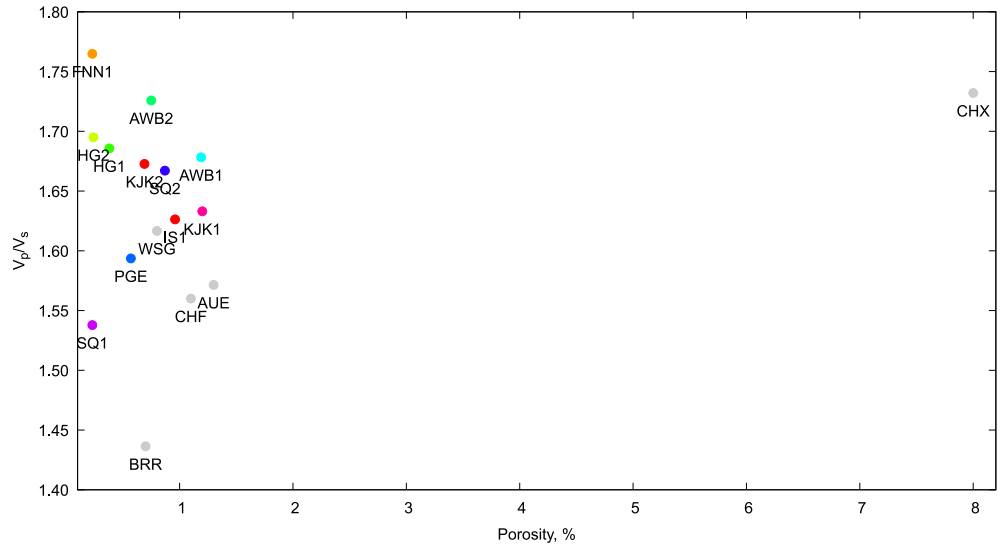

Figure 3. Ratio of V_p and V_s compared to porosity. Note that samples AUE, WSG, CHF, and BRR are reference samples of unshocked granite, and CHX is a sample from the upper peak ring of the Chicxulub impact structure. All control samples are plotted in gray.

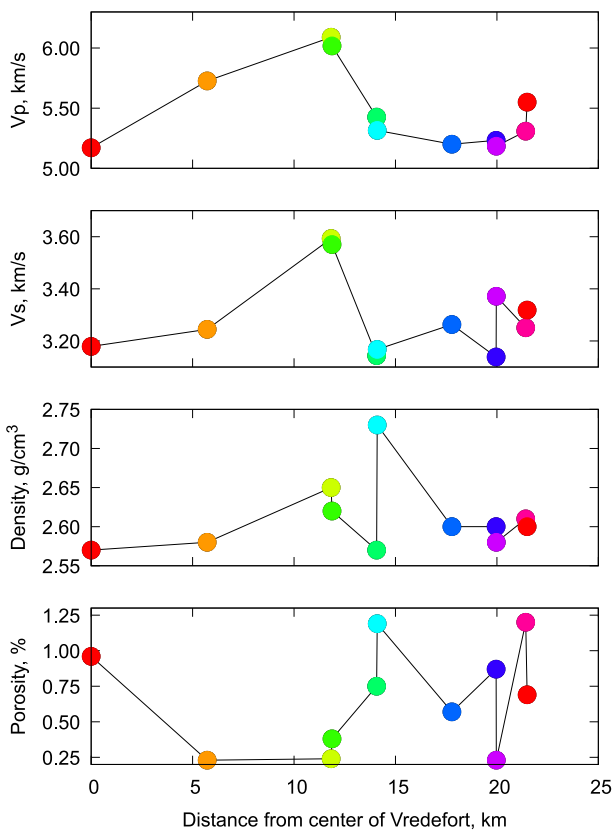

Figure 4. Comparison of measured properties with distance from the center of the Vredefort structure. Color-coding of symbols as in Figure 3. Note that all samples were taken within the core of the structure.

composition of Vredefort Granophyre, containing a groundmass of fine intergrowths of pyroxene laths and plagioclase, with quartz-rich xenolithic inclusions that preserve shock features. The impact melt rock FNN-2 is broadly similar to xenolithic inclusions within a granophyric textured groundmass.

4.2. Rock Properties

The measured physical properties, along with the precise locations of the samples and the corresponding Bouguer anomaly at the sites where the samples were taken, are summarized in Table 1. At the Inlandsee, the porosity is 0.96%, decreasing to 0.24% at 11.9 km distance. The maximum porosity values were at 13.8 (1.19%) and 21.5 km (1.20%) (Figure 3). The V_p of the samples ranges from 5.17 to 6.09 km/s. Between 0 and 11.9 km from the center of the structure, V_p increases from 5.17 to 6.09 km/s, but from 13.8 to 21.5 km distance, V_p decreases to a range between 5.18 and 5.55 km/s (Figure 4). The V_s of the samples range from 3.14 to 3.59 km/s. From 0 to 11.9 km, relative to the center of the structure, the V_s increases from 3.18 to 3.59, and from 13.8 to 21.5 km, V_s fluctuates from 3.14 to 3.37 km/s (Figure 4). The porosity of the samples ranges from 0.23% to 1.20%.

4.3. Matlab Modeling

The results of the calculations are summarized in Table 2, as well as Figures S1–S4 and Table S1 in Supporting Information S1. All of the measured grain and rock densities are either within the calculated bounds or have a difference of less than 2% from the nearest calculated value (Figure 5). The highest mismatches are for samples IS1, HG2, and AWB2 where the density is lower than the lowest calculated value. The measured density of IS1 is 2.57 g/cm^3, and the calculated density averages 2.635 g/cm^3. The measured density of HG2 is 2.65 g/cm^3, and its calculated density averages 2.704 g/cm^3. The measured density of AWB2 is 2.57 g/cm^3, and the calculated density averages 2.619 g/cm^3. All five test samples have densities within the calculated bounds

Journal of Geophysical Research: Planets

10.1029/2022JE007721

Table 2
Calculated Results for Each Sample and the Reference Materials

Sample	Distance (km)	Rho grains min (g/cm^3)	Rho grains max (g/cm^3)	Rho min (g/cm^3)	Rho max (g/cm^3)	V_p Reuss min (km/s)	V_p Reuss max (km/s)	V_p Voigt min (km/s)	V_p Voigt max (km/s)	V_p VRH min (km/s)	V_p VRH max (km/s)	V_s Voigt min (km/s)	V_s Voigt max (km/s)	V_s VRH min (km/s)	V_s VRH max (km/s)	Rho grains (g/cm^3)	Rho (g/cm^3)	V_p (km/s)	V_s (km/s)
IS1	0	2.62	2.70	2.60	2.67	0.06	0.06	6.03	6.62	4.26	4.68	3.61	3.87	2.56	2.73	2.60	2.57	5.17	3.18
FNN2	5.7	2.65	2.77	2.65	2.76	0.13	0.12	5.86	6.57	4.15	4.65	3.52	3.95	2.49	2.79	2.66	2.65	6.09	3.59
FNN1	5.7	2.59	2.65	2.59	2.65	0.13	0.13	5.98	6.34	4.23	4.48	3.52	3.69	2.49	2.61	2.61	2.58	5.73	3.25
HG1	11.7	2.61	2.66	2.60	2.65	0.10	0.10	6.01	6.33	4.25	4.48	3.56	3.72	2.51	2.63	2.64	2.62	6.02	3.57
HG2	11.7	2.72	2.70	2.71	2.70	0.12	0.12	6.17	6.58	4.36	4.65	3.64	3.87	2.57	2.74	2.66	2.65	6.09	3.59
AWB1	14.1	2.82	2.79	2.78	2.75	0.05	0.06	6.28	6.85	4.44	4.84	3.58	3.89	2.53	2.75	2.78	2.73	5.32	3.17
AWB2	14.1	2.62	2.65	2.60	2.63	0.07	0.07	6.00	6.15	4.24	4.35	3.85	3.93	2.72	2.78	2.60	2.57	5.43	3.14
PGE	17.6	2.62	2.70	2.61	2.69	0.08	0.08	5.94	6.50	4.20	4.60	3.61	3.88	2.55	2.74	2.62	2.60	5.20	3.26
SQ1	19.8	2.61	2.67	2.60	2.66	0.13	0.13	6.01	6.37	4.25	4.51	3.63	3.81	2.56	2.70	2.62	2.58	5.18	3.37
SQ2	19.8	2.61	2.67	2.59	2.65	0.07	0.07	6.01	6.40	4.25	4.52	3.62	3.81	2.56	2.70	2.62	2.60	5.23	3.14
KJK1	21.4	2.62	2.70	2.58	2.67	0.06	0.06	5.94	6.39	4.20	4.52	3.61	3.87	2.55	2.74	2.66	2.61	5.31	3.25
KJK2	21.4	2.63	2.70	2.61	2.68	0.07	0.07	5.95	6.36	4.21	4.50	3.57	3.79	2.53	2.68	2.64	2.60	5.55	3.32
AUE*	Reference	2.61	2.72	2.58	2.68	0.05	0.05	5.95	6.53	4.21	4.62	3.50	3.82	2.48	2.70	2.65	2.62	4.95	3.15
WSG*	Reference	2.62	2.71	2.60	2.69	0.07	0.07	6.01	6.53	4.25	4.61	3.49	3.76	2.47	2.66	2.66	2.64	4.85	3.00
CHF*	Reference	2.60	2.68	2.57	2.65	0.06	0.06	5.92	6.26	4.19	4.43	3.53	3.73	2.49	2.64	2.63	2.61	3.90	2.50
BRR*	Reference	2.66	2.77	2.64	2.75	0.07	0.07	5.96	6.66	4.22	4.71	3.45	3.85	2.44	2.72	2.65	2.64	3.95	2.75
CHX*	Reference	2.66	2.75	2.45	2.53	0.02	0.02	5.83	6.60	4.12	4.67	3.36	3.83	2.38	2.71	2.68	2.47	4.10	2.37

Note. The * represents reference samples.

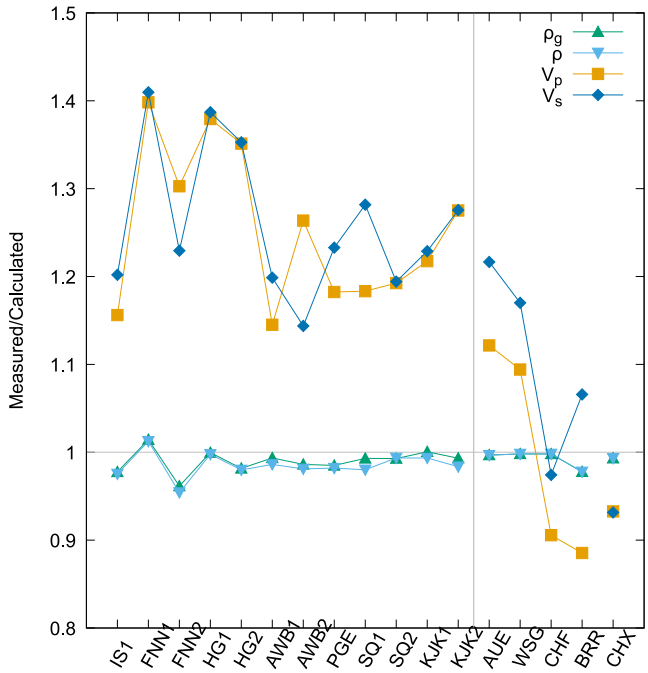

Figure 5. Measured values of grain density, density, *P*- and *S*- velocity normalized to calculated theoretical values (Table 2). Note that samples AUE, WSG, CHF, and BRR are reference samples of unshocked granite, and CHX is a sample from the upper peak ring of the Chicxulub impact structure.

except for sample BRR, whose density is 0.3% below the lowest calculated value. The calculated and measured densities, therefore, are similar.

All calculated *P*- and *S*- wave velocities are lower than those calculated using the upper Voigt bound, representing the maximum possible values of an aggregate. The Voigt-Reuss-Hill average (VRH) *P*- and *S*- wave velocities for the five test samples agree well with the measured values. The highest mismatches are those of samples AUE and CHF, whose measured *P*-wave velocities are ∼10% higher and ∼8% lower than the VRH bounds. The *S*-wave velocities for samples AUE and WSG are ∼15% higher than the VRH bounds. All the other test samples have *S*-wave velocities within or very close to the VRH bounds (Figure 5). The *P*- and *S*-wave velocities for our samples are ∼10%–∼40% higher than the VRH velocities. In particular, samples FNN2, FNN1, HG1, and HG2 have measured velocities that are 25%–40% higher than the VRH values. Such samples are all clustered around the center of the impact crater and are those presenting the highest melt portion. Sample IS1, which is at the crater center, and the samples farther away from the impact crater center (AWB1, AWB2, PGE, SQ1, SQ2, KJK1, and KJK2) present velocities ∼20% higher than the VRH values (Table 2).

4.4. Gravity

The Bouguer gravity anomaly of the Vredefort Structure can only be distinguished from the surrounding terrane within the area of the Vredefort Dome (Figure 6a). The NW of the Dome has a gravity high of −95 mGal, with a broad peak that extends across 37 km. The area south of the Bushveld Complex, 135 km radially from the center of the Vredefort structure, has a gravity low of −180 mGal. The slope of gravity demonstrates that the gravity anomaly immediately surrounding the Vredefort Dome is related to the structure, but the surrounding gravity lows are unlikely to be related to Vredefort (Figure 6b). A trough has a localized gravity low of −130 mGal, and the center of the Dome has a peak of −120 mGal. The SW of the structure has a gravity low of −140 mGal (Figure 6c). Overall, the Kaapvaal Craton has a Bouguer anomaly ranging from approximately −30 to −190 mGal (Figure 7). The most positive anomalies on the Kaapvaal craton are associated with the Bushveld Complex and the Trompsburg layered igneous intrusion, each having Bouguer gravity anomalies of −50 to −30 mGal (Westgate et al., 2022). The lowest anomalies on the Kaapvaal craton are associated with thick sediments of the Karoo Supergroup, causing Bouguer gravity anomalies as low as −180 mGal. The southern margin of the Bushveld Complex has similarly low gravity anomalies, likely related to warping of the Moho caused by the large intrusive mass of the Bushveld Complex (Webb et al., 2004).

There is no obvious correlation between the Bouger gravity anomalies field areas selected in this study and the measured properties of the samples (Table 1). Based on the lack of correlation, it is unlikely that there is a controlling factor between the measured physical properties and the gravity data.

4.5. Numerical Modeling

The iSALE simulation of the Vredefort impact event has minor variations with the original SALEB simulation of Ivanov (2005). Here, the crater has a final rim-to-rim diameter of 152 km compared to 172 km (Figure 8a). At 8–10 km depth in the model, metamorphosed sedimentary rocks occur from radial distances of ∼24 km, consistent with the expected amount of post-impact erosion and the present-day boundary between the collar and core of the Vredefort Dome. At 8–10 km depth, the simulation predicts an increase in porosities immediately after crater formation in the core at less than 0.4% (Figure 8b). In the collar, porosities may have increased by 4.5% (Figure 8b); however, it is important to note that the upper crustal layer was assumed to have no initial porosity. Higher initial porosities would result in a lower magnitude of impact-generated porosity.

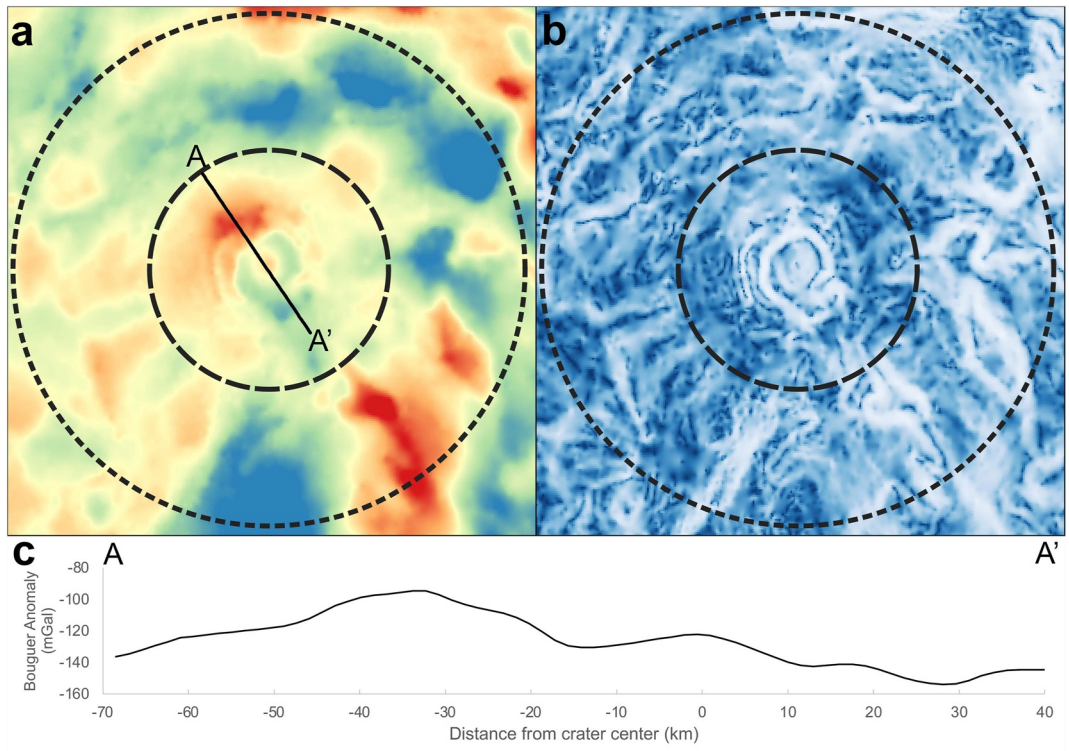

Figure 6. (a) Gravity anomaly of the Vredefort impact structure. Gravity highs are located near the collar of the Vredefort Dome and in the center of the Dome. Line indicates the location of the profile shown in panel (c). (b) Slope of gravity of the Vredefort impact structure ranging from 0 (blue) to 90 (white). Note that the Vredefort Dome is clearly definable in this projection. Values were calculated. (c) Gravity profile through the Vredefort Dome along A-A′. A broad gravity high is still present. Data from the South African Council for Geoscience.

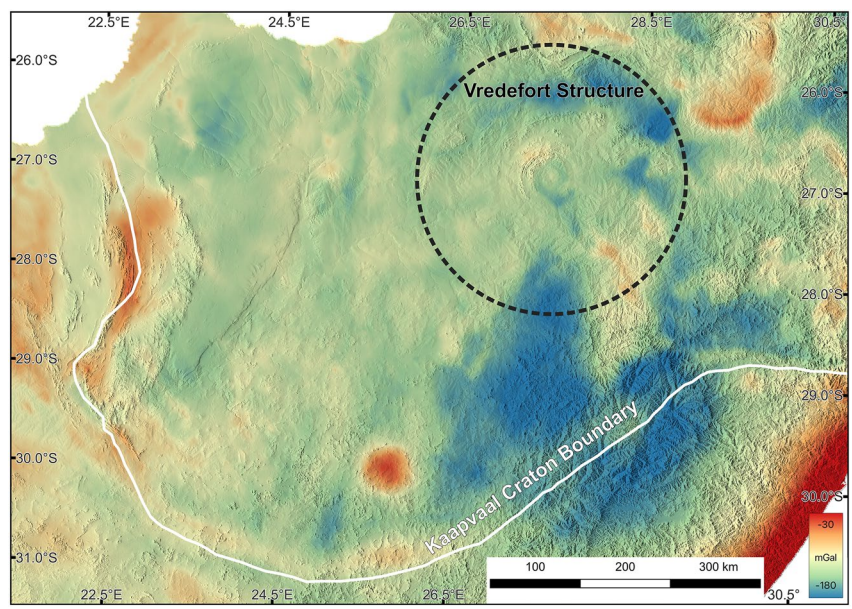

Figure 7. Gravity map of the Kaapvaal Craton. The Vredefort structure does not have a prominent gravity high or low compared to the surrounding craton. Data from the South African Council for Geoscience. Craton boundary from Hasterok et al. (2022).

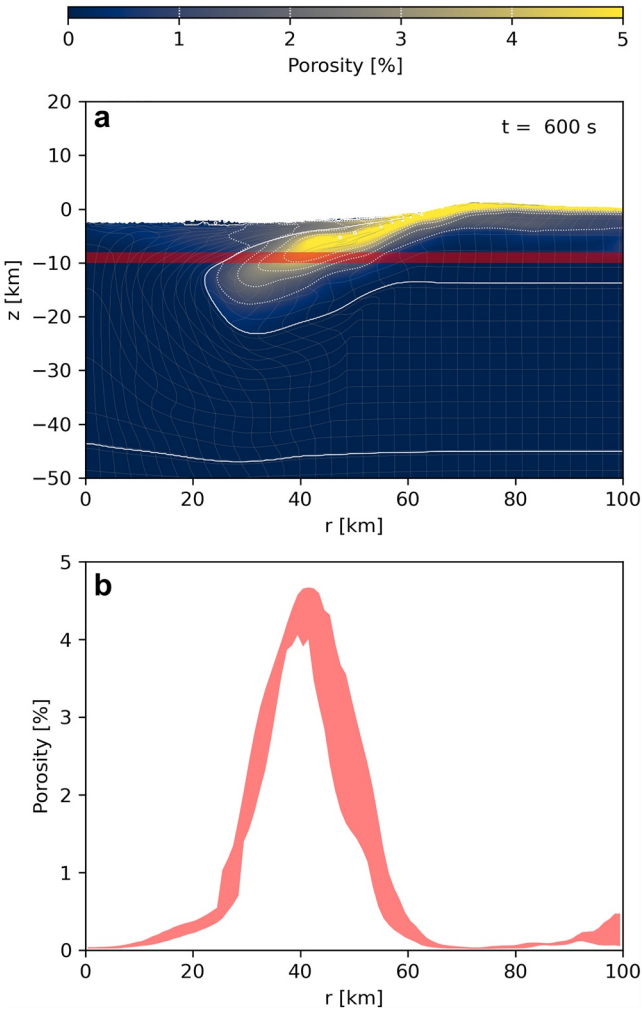

Figure 8. (a) Final timestep of iSALE simulation of the Vredefort impact event. At this time, major cratering motions have ceased. Porosity in the target is color-shaded and contoured. (b) Radial profile of porosity in the simulation at 8–10 km depth. The shaded region indicates the range of porosities in this depth interval.

5. Discussion

5.1. Comparison of Vredefort With Chicxulub

In order to establish the preservation potential of a large impact structure, it is necessary to compare a deep transect through an impact structure with a fully preserved, similarly sized impact structure. The erosional profile of the Vredefort impact structure permits a geological transect to be taken through the exposed surface rocks. Of the three known basin-scale impact structures in the world, Vredefort is the only one that exposes the buried central uplift to be studied directly in the field. Chicxulub, by contrast, is a near-pristine basin-sized impact structure. Furthermore, the recent work on the Chicxulub impact structure surrounding the ICDP-IODP drilling project 364 has produced a wealth of data that can permit an updated comparison between Vredefort and Chicxulub to be made, despite the 1.95 Ga age difference between the impact structures. Many of the features of the two impact structures are similar and can be directly related to one another.

The size of the Vredefort structure has been debated for decades. An early estimate by Dietz (1961) suggested a size as small as 40 km, as he only considered the inner part of the Vredefort Dome to represent the impact structure, but later workers suggested a size up to 300 km based on seismic profiles, fault analysis, and scaling estimations based on the peak ring size (Therriault et al., 1996; Turtle et al., 2003). Numerical modeling of the Vredefort structure has suggested a diameter of 180 km (Ivanov, 2005). Similarly, Chicxulub has been estimated to be between 160 and 200 km in diameter (Collins et al., 2008, 2020; Gulick et al., 2008, 2013; Morgan et al., 2016; Rae et al., 2019a, 2019b). A direct comparison between the Vredfort and Chicxulub structures was made by R. A. F. Grieve et al. (2008), who considered that the individual structural features of the impact structures were indistinguishable, and considered the structures to be approximately of the same size (e.g., R. Grieve & Therriault, 2000; R. A. F. Grieve et al., 2008).

Comparable major structural features are present at both Vredefort and Chicxulub (Figure 9). Vredefort preserves the hinge zone below the supracrustal sequence that likely indicates rocks that were below the peak ring with a radial distance of 30–35 km from the center of the structure. The Potchefstroom fault has a radial distance of 70 km, and the Rand Anticline and thrust zone is located at a radial distance of ca. 115 km from the center of Vredefort (Friese et al., 1995). At Chicxulub, major crustal-scale faults are observed at a similar radial distance of 75 km, and the exterior ring faults are at approximately 125 km (Gulick et al., 2013). Seismic profiles of these structures at Chicxulub show that they dip toward the center of the structure, suggesting that erosion should reduce the radial profile of the structure. Most of the Chicxulub structural effects do not extend below a depth of 10 km, although whole crustal faulting is inferred for the inner rim faults (Gulick et al., 2013) and the Moho is upwarped beneath the buried central uplift by 1–2 km (Christeson et al., 2009; Gulick et al., 2013). A reasonably strong correlation can be made between the observed features at Vredefort and the deep features at Chicxulub at a depth of 8–9 km (R. Grieve & Therriault, 2000), possibly suggesting an independent evaluation of the erosional depth of Vredefort.

Apart from similarities, there are a few differences. The target of Vredefort was cratonic crust overlain by a thick supracrustal sequence (i.e., >10 km), as opposed to Chicxulub, where the asteroid impacted relatively young continental crust with a moderate thickness of supracrustal sediments (i.e., <3 km). The two impact structures provide two different views of processes occurring in basin-sized impacts: the pre-impact depth of the Vredefort samples is likely 25–30 km (Figure 8), a significantly greater depth than the peak-ring samples that have been analyzed at Chicxulub, which had a pre-impact depth of 10 km (Morgan et al., 2016).

The difference in erosional level between Vredefort and Chicxulub affects the physical properties of the rocks that crop out or are accessible by drilling in both structures. The samples from the upper part of the Chicxulub peak

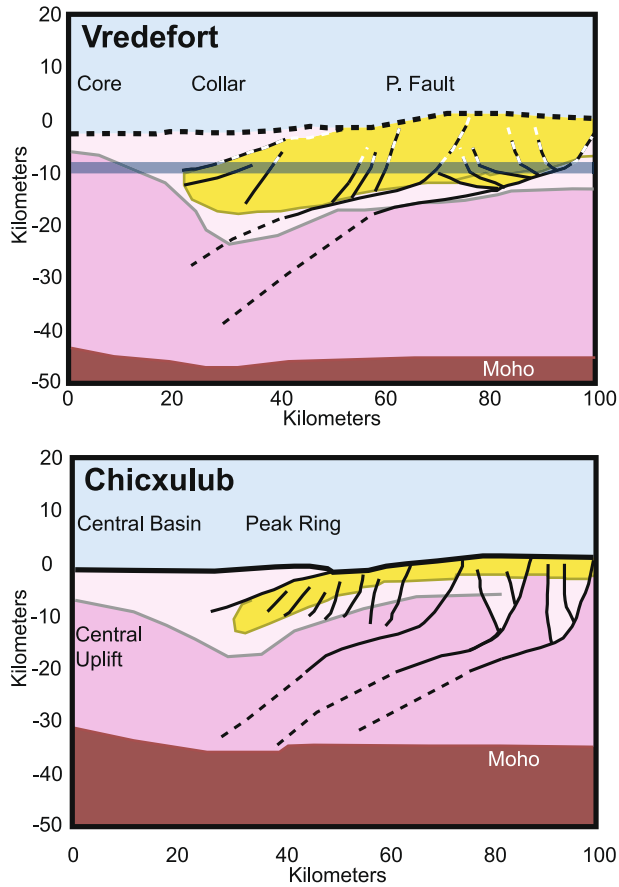

Figure 9. Representations of Vredefort and Chicxulub craters in half-space, set at the same scale for comparison. Topography and general structure of Moho and crustal and surface topography from hydrocode models scaled to geophysical data. Fault representations modified from seismic reflection data interpretations for Chicxulub (Gulick et al., 2008) and Vredefort (Friese et al., 1995). Crater surface is shown as a thick black line (broken line for Vredefort), faults as thin black lines, approximate contour for sediments/supracrustal section shown in yellow. All lines dashed were inferred at depth or projected above the erosion level to the original crater surface. Depth of erosion for Vredefort is shown as a blue band (8–10 km). Note that similarly the scale of the impact structures and correlation of the collar at Vredefort with the peak ring at Chicxulub, with the difference being the depth of erosion. P. Fault = Potchefstroom Fault.

ring are strongly distinct from the expected values for the sampled lithologies, for example, the Chicxulub granitoids have >10% porosity, 2.1 g/cm^3 density, and 4 km/s V_p (Christeson et al., 2018), while unaffected granitoids have porosity <1%, density of 2.65 g/cm^3, and V_p of 5.5 km/s. In contrast, the physical properties of the measured Vredefort samples in this study are within error of the expected values of equivalent lithologies unaffected by shock metamorphism, and from the theoretically calculated values for these samples, with the exception of velocity (Table 1). Velocities for Vredefort samples are higher than for equivalent unshocked lithologies, the cause of which may be domains of impact melt rock, depth of origination of these rocks due to the unroofing provided by the impact, or the combined effects of impact and burial. Greater physical property changes that may have occurred to the samples were potentially eliminated through re-equilibration as the rocks might have remained buried at depth after the impact for at least 1 Ga (Kovaleva et al., 2019; Moser et al., 2011). Therefore, the geophysical characteristics of individual samples leave few methods for conclusively identifying an impact event from physical properties alone, with the potential exception of melt rock and its high V_p/V_s ratio. This is consistent with the geophysical signature of impact melt (high V_p, high V_p/V_s ratio, low permeability) being detectable in a variety of geophysical techniques (i.e., Fourie et al., 2019), and may indicate that impact structures remain potentially detectable by geophysical methods even in the subsurface, provided that a significant amount of impact melt is preserved.

Previous analysis of gravity signatures of impact craters has shown that as crater size increases, the magnitude of the gravity response increases until it reaches its maximum. After that point, the value remains at the maximum and only the diameter of the gravity response increases. The principal factors determining the gravity signature of an impact structure are the changes in the geophysical properties of the rocks in the upper 10 km of the structure and the uplift of the mantle below the crater (Pilkington & Grieve, 1992). The gravity signature of the Vredefort impact structure has a much lower magnitude than other gravity anomalies within the Kaapvaal Craton that are attributed to tectonic structures (Figure 7). The remaining gravity anomalies at Vredefort are probably controlled by a combination of the remnants of material that was underthrust beneath the peak ring (i.e., the supracrustal sequence) and the uplifted Moho beneath the Vredefort Structure (Youssof et al., 2013). At Chicxulub, changes in the physical properties of the rocks can be correlated with geophysical data (Christeson et al., 2018; Rae et al., 2019a, 2019b) as the increased porosity and decreased density of the shocked target rocks decrease the density and velocity within the upper stratigraphic levels of the structure.

5.2. Potential for Discovery of Archean Impact Structures

The Archean Eon represents a time of substantial crustal growth, including the formation and growth of greenstone belts and cratons and the potential onset of modern plate tectonic processes (e.g., Voice et al., 2011). Older greenstone belts and tonalite-trondhjemite-granodiorite (TTG) intrusions provided the cores of the cratons. Many impact ejecta horizons are known from greenstone belts, and have been interpreted to represent the largest known impact events. Additionally, preserved greenstone belts are typically strongly deformed and folded due to the intrusion of surrounding TTGs both deforming and preserving the greenstone belts. The greatest growth of the continental crust occurred at ca. 2.7 Ga, meaning that there is only a 200 Ma window between the extensive growth of the Archean cratons and the Archean-Proterozoic boundary. However, the physical process of impact crater formation should not have differed. Any differences in the Archean atmosphere or surficial processes would not affect the deep portions of an impact structure that could still be theoretically preserved. To understand

the potential of Archean impact structures to be preserved, it is necessary to examine the oldest Proterozoic impact structures.

Vredefort is one of the three oldest impact structures known, with the Yarrabubba structure having a suggested age of 2.23 Ga, and the Sudbury structure being 1.85 Ga. Each of these impact structures is significantly younger than the Archean-Proterozoic boundary. The Yarrabubba structure has an age constrained by the older 2.6 Ga monzogranites of the target rocks (Macdonald et al., 2003), and regional dolerite dikes that cross-cut the Yilgarn Craton that are dated between approximately 1.5 and 1.0 Ga (Pirajno & Hoatson, 2012). Shocked zircons and monazites from the structure have been dated to ca. 2.23 Ga (Erickson et al., 2020) based on two samples. The structure is deeply eroded but still preserves some thin pseudotachylites and shatter cones. The original size of the structure is poorly constrained but is assumed to be between 35 and 70 km (Erickson et al., 2020; Macdonald et al., 2003). It is unclear to what depth the structure has been eroded, as few outcrops of the structure are preserved on the surface. The Sudbury structure is approximately 170 Ma younger than Vredefort and experienced a radically different tectonic history, being folded due to the Penokean Orogeny shortly after the impact occurred, burying major portions of the melt sheet deeply into the subsurface (Lightfoot et al., 1997). Despite the large amount of erosion that the Sudbury structure has experienced, the unusual tectonic deformation allows for the preservation of impact features. The original size of the Yarrabubba structure is not well understood, but the Sudbury and Vredefort structures are remnants of the two largest preserved impact structures on Earth.

Although Vredefort represents the remnants of the largest terrestrial impact event for which an impact structure is preserved, the 10 km of erosion that the structure has experienced has eliminated most of the defining geophysical evidence of the impact event. There are no geophysical properties of the Vredefort structure that distinguish it from surrounding rocks, with the exception of the circularity of the anomaly pattern. The physical properties of the basement rocks are indistinguishable from unshocked rocks with the exception of a slight velocity increase above the expected, which may reflect the depth of origination of the rocks within the Vredefort Dome. The impact melt-rich samples also show a high V_p/V_s ratio. The gravity signature of Vredefort does not correlate with any of the physical properties measured in this study, and is most likely not controlled by shallow surface properties but rather by deeper features, such as the uplift of the Moho. The Bouguer anomaly of Vredefort is smaller than the anomalies of other geological features surrounding the impact structure (Figure 7). If the Vredefort structure in its present form were fully buried (e.g., by the Karoo sediments that cover the southern half of the structure), it would be exceptionally difficult to identify its presence from geophysical data.

The only types of evidence of impact that are still preserved at Vredefort are shocked minerals and high-pressure polymorphs with localized occurrences (e.g., Kovaleva & Habler, 2019; Kovaleva et al., 2019; Martini, 1978), shatter cones (also localized), and shallow remnants of the impact melt (Clark et al., 2021; Fourie et al., 2019). The shocked minerals in Vredefort are now well established, and include high-pressure phases such as coesite and stishovite (Martini, 1978), as well as shocked minerals, including PDFs and PFs in quartz (French et al., 1989), and microtwins and granular textures in zircon and monazite (e.g., Kamo et al., 1996; Kovaleva & Habler, 2019; Kovaleva et al., 2019; Moser et al., 2011). However, these features are best preserved locally, for example, within or around pseudotachylites or within the Vredefort Granophyre Dikes. The shock features in quartz are often recrystallized to the extent that they are debatable (e.g., Figure 2a). In the 1980s and 1990s, these features were observed by numerous workers who determined that they were not shock features (e.g., Reimold, 1990). The rocks experienced burial at a depth of 10 km after the impact event, and the geothermal gradient at such depths is sufficient to allow recrystallization and re-equilibration of many of the rock-forming minerals. What remains of shocked minerals may be removed by further erosion or easily hidden by burial of the impact structure. Shocked minerals are widely considered the most reliable form of evidence of shock metamorphism, but by their nature they require microstructural analysis. Remote sensing surveys or geophysical surveys that often allow for the initial discovery of a candidate impact structure will not reflect this type of evidence.

These observations provide a potential upper bound on the depth of erosion beyond which the evidence of an impact event is removed. The Vredefort Granophyre Dikes in the core of the structure have been demonstrated to be preserved at their lowermost extent based on electrical resistivity studies as well as a fortuitous trench that was produced adjacent to a Granophyre dike, confirming the depth extent (Clark et al., 2021; Fourie et al., 2019; Huber et al., 2022). A further 0.01 km of erosion would likely remove all of the dikes in the core of the central uplift, erasing one of the only remaining geophysical/physical property signatures (impact melt velocity). It is unknown to what depth pseudotachylites are preserved. Quarries, such as the sampled Salvamento quarry, extend

10–20 m below the present day surface, and pseudotachylites are locally exposed in the deepest floor rocks. Further erosion will remove the evidence of these melt rocks in the crystalline basement rocks, and possibly only a moderate amount of erosion will be required.

The supracrustal sequence that is around the crystalline basement originally lay beneath the peak ring of Vredefort and has a modern depth extent of about 1 km (Molezzi et al., 2019); therefore, it may be expected that a further 1 km of erosion would remove most evidence of shock metamorphism contained in these rocks. The slight velocity increase present relative to similar lithologies would not be diagnostic of an impact without other clear indicators such as shocked and impact melt rocks. The length of time that the impact structure will continue to be observable depends on the erosion rate. Large-scale impact structures (i.e., >100 km diameter) typically cause extensive areas of structural uplift and brecciation around and below the impact structure. As has been seen in the peak ring of the Chicxulub impact structure, the rocks in the upper peak ring are weakened by the impact process, and the changes in physical properties generally cause the rocks to be more easily subjected to erosion. The impact melt sheet, by contrast, is a crystalline rock that would resist erosion. Once the impact melt sheet is removed, the weakened, brecciated rocks below the melt sheet can potentially be rapidly eroded. The zone of brecciation would extend down to the level in the crust where the fractures would be annealed. Therefore, an impact structure may experience relatively slow erosion soon after it forms until the melt sheet is penetrated, followed by rapid erosion while the brecciated zone is removed, and then slow erosion in the deep basement. Global observations suggest that the median erosion rate for drainage basins would be approximately 50 m/Myr, whereas stable outcrops may have low median erosion rates of 5 m/Myr, providing a range of endmember values to consider (Portenga & Bierman, 2011). At an average erosional rate of 50 m/Myr, 1 km of erosion could happen within 20 Myr; at 5 m/Myr, this could occur within 200 Myr. Based on the evidence from Vredefort, even the largest craters may be undetectable if they experience >10 km of erosion. At even modest erosional rates of 5 m/Ma, 10 km of erosion would occur within 2 Gyr. We predict that any existing impact structure older than 2 Ga must have experienced unusual preservation, and any crater, regardless of initial size, will be removed from the geological record once eroded beyond 10 km depth. It is currently unclear to what depth the Yarrabubba structure has been eroded, and further study of that structure may provide additional insights into the characteristics needed to allow the preservation of old impact structures. To find Archean impact structures, it is necessary to search in cratons where small amounts of erosion have taken place.

6. Conclusions

1. The measurable geophysical properties of samples at Vredefort are statistically indistinguishable from unshocked rocks with the exception of a small velocity increase compared to reference materials where impact melt rock is present.
2. The gravity anomaly observed at Vredefort is controlled by deeper features rather than shallow characteristics of the target rocks.
3. Vredefort is structurally remarkably similar to Chicxulub at a depth of 8–9 km, which suggests that the two structures have similar original sizes.
4. A further ca. 1 km of erosion of Vredefort, which could happen in as little as 20 Myr, would result in a loss of evidence that the structure is impact-related.
5. Any impact structure on Earth, if eroded below 10 km depth, will be difficult or impossible to identify.
6. Archean impact structures can only be recognized if they are in areas of unusual preservation.

Data Availability Statement

Plotting of data was performed using Gnuplot 5.4 (http://www.gnuplot.info/). Maps were generated using QGIS 3.28 (https://www.qgis.org/). Data for gravity and geology of South Africa are available from the South African Council for Geoscience (https://www.geoscience.org.za/index.php/publication/downloadable-material). iSALE is not currently available to the public and is accessible to the impact community on a case-by-case basis for non-commercial use. Details of iSALE access are available at https://isale-code.github.io/. Data sets for input files can be found in Huber et al. (2023). All other data and software used in this study can be found in the Methods section and Supporting Information S1.

Acknowledgments
The authors wish to thank Mr. Christo Meyer for his assistance with access to field sites in and around Vredefort and for his continued support of geoscience research. We also thank Dr. Martin Clark for assistance in sample collection. Funding for this research was provided by the Incentive Funding for Rated Researchers by the National Research Foundation of South Africa, RA181101385896. ASPR gratefully acknowledges funding from Trinity College, University of Cambridge. This is the University of Texas Institute for Geophysics Contribution 3960 and Center for Planetary Systems Habitability Contribution 0066. The authors wish to thank Boris Ivanov and Aaron Cavosie for their insightful and constructive reviews.

References

Amsden, A. A., Ruppel, H. M., & Hirt, C. W. (1980). SALE: A simplified ALE computer program for fluid flow at all speeds. https://doi.org/10.2172/5176006

Benz, W., Cameron, A. G. W., & Melosh, H. J. (1989). The origin of the Moon and the single-impact hypothesis III. *Icarus*, *81*(1), 113–131. https://doi.org/10.1016/0019-1035(89)90129-2

Birch, F. (1960). The velocity of compressional waves in rocks to 10 kilobars: 1. *Journal of Geophysical Research*, *65*(4), 1083–1102. https://doi.org/10.1029/JZ065i004p01083

Bisschoff, A. A. (1972). The dioritic rocks of the Vredefort Dome. *South African Journal of Geology*, *75*(1), 31–45.

Brace, W. F. (1965). Some new measurements of linear compressibility of rocks. *Journal of Geophysical Research*, *70*(2), 391–398. https://doi.org/10.1029/JZ070i002p00391

Byerly, G. R., Lowe, D. R., Wooden, J. L., & Xie, X. (2002). An Archean impact layer from the Pilbara and Kaapvaal cratons. *Science*, *297*(5585), 1325–1327. https://doi.org/10.1126/SCIENCE.1073934/

Cavosie, A. J., Erickson, T. M., Montalvo, P. E., Prado, D. C., Cintron, N. O., & Gibbon, R. J. (2017). The Rietputs Formation in South Africa: A Pleistocene fluvial archive of meteorite impact unique to the Kaapvaal craton. *Microstructural Geochronology: Planetary Records Down to Atom Scale*, 203–224. https://doi.org/10.1002/9781119227250.CH9

Cawthorn, R. G., & Walraven, F. (1998). Emplacement and crystallization time for the Bushveld complex. *Journal of Petrology*, *39*(9), 1669–1687. https://doi.org/10.1093/PETROJ/39.9.1669

Christeson, G. L., Collins, G. S., Morgan, J. V., Gulick, S. P. S., Barton, P. J., & Warner, M. R. (2009). Mantle deformation beneath the Chicxulub impact crater. *Earth and Planetary Science Letters*, *284*(1–2), 249–257. https://doi.org/10.1016/j.epsl.2009.04.033

Christeson, G. L., Gulick, S. P. S., Morgan, J. V., Gebhardt, C., Kring, D. A., le Ber, E., et al. (2018). Extraordinary rocks from the peak ring of the Chicxulub impact crater: P-Wave velocity, density, and porosity measurements from IODP/ICDP expedition 364. *Earth and Planetary Science Letters*, *495*, 1–11. https://doi.org/10.1016/j.epsl.2018.05.013

Clark, M. D., Kovaleva, E., Huber, M. S., Fourie, F., & Harris, C. (2021). Post-impact faulting of the Holfontein granophyre dike of the Vredefort impact structure, South Africa, inferred from remote sensing, Geophysics, and geochemistry. *Geosciences*, *11*(2), 96. https://doi.org/10.3390/geosciences11020096

Collins, G. S. (2014). Numerical simulations of impact crater formation with dilatancy. *Journal of Geophysical Research: Planets*, *119*(12), 2600–2619. https://doi.org/10.1002/2014JE004708

Collins, G. S., Melosh, H. J., & Ivanov, B. A. (2004). Modeling damage and deformation in impact simulations. *Meteoritics & Planetary Sciences*, *39*(2), 217–231. https://doi.org/10.1111/J.1945-5100.2004.TB00337.X

Collins, G. S., Melosh, H. J., & Wünnemann, K. (2011). Improvements to the ε-α porous compaction model for simulating impacts into high-porosity solar system objects. *International Journal of Impact Engineering*, *38*(6), 434–439. https://doi.org/10.1016/J.IJIMPENG.2010.10.013

Collins, G. S., Morgan, J., Barton, P., Christeson, G. L., Gulick, S., Urrutia, J., et al. (2008). Dynamic modeling suggests terrace zone asymmetry in the Chicxulub crater is caused by target heterogeneity. *Earth and Planetary Science Letters*, *270*(3–4), 221–230. https://doi.org/10.1016/J.EPSL.2008.03.032

Collins, G. S., Patel, N., Davison, T. M., Rae, A. S. P., Morgan, J. V., Gulick, S. P. S., et al. (2020). A steeply-inclined trajectory for the Chicxulub impact. *Nature Communications*, *11*(1), 1–10. https://doi.org/10.1038/s41467-020-15269-x

Coyner, K. B. (1984). *Effects of stress, pore pressure, and pore fluids on bulk strain, velocity, and permeability in rocks*. PhD Thesis, Massachusetts Institute of Technology.

Dietz, R. S. (1961). Vredefort ring structure: Meteorite impact scar? *The Journal of Geology*, *67*(5), 499–516. https://doi.org/10.1086/626768

Durrheim, R. J., Nicolaysen, L. O., & Corner, B. (1991). A deep seismic reflection profile across the Archean-Proterozoic Witwatersrand basin, south Africa. *Geodynamics*, *22*, 213–224. https://doi.org/10.1029/GD022P0213

Erickson, T. M., Kirkland, C. L., Timms, N. E., Cavosie, A. J., & Davison, T. M. (2020). Precise radiometric age establishes Yarrabubba, Western Australia, as Earth's oldest recognised meteorite impact structure. *Nature Communications*, *11*(1), 1–8. https://doi.org/10.1038/s41467-019-13985-7

Farr, T. G., & Kobrick, M. (2000). Shuttle radar topography mission produces a wealth of data. *Eos, Transactions American Geophysical Union*, *81*(48), 583. https://doi.org/10.1029/eo081i048p00583

Flowers, R. M., Moser, D. E., & Hart, R. J. (2003). Evolution of the Amphibolite-granulite facies transition exposed by the Vredefort impact structure, Kaapvaal craton, South Africa. *The Journal of Geology*, *111*(4), 455–470. https://doi.org/10.1086/375282

Fourie, F. D., Huber, M. S., & Kovaleva, E. (2019). Geophysical characterization of the Daskop granophyre dyke and surrounding host rocks, Vredefort impact structure, South Africa. *Meteoritics & Planetary Sciences*, *54*(7), 1579–1593. https://doi.org/10.1111/maps.13300

French, B. M., Orth, C. J., & Quintana, L. R. (1989). Iridium in the Vredefort Bronzite Granophyre-Impact melting and limits on a possible extraterrestrial component. In *Lunar and planetary science conference proceedings* (Vol. 19, pp. 733–744).

Friese, A. E. W., Charlesworth, E. G., & McCarthy, T. S. (1995). *Tectonic processes within the Kaapvaal Craton during the Kibaran (Grenville) Orogeny: Structural, geophysical, and isotopic constraints from the Witwatersrand basin and environs*. Information Circular (Vol. 292, pp. 1–67). University of the Witwatersrand.

Gibson, R. L., Reimold, W. U., & Stevens, G. (1998). Thermal-metamorphic signature of an impact event in the Vredefort dome, South Africa. *Geology*, *26*(9), 787–790. https://doi.org/10.1130/0091-7613(1998)026<0787:TMSOAI>2.3.CO;2

Grieve, R., & Therriault, A. (2000). Vredefort, Sudbury, Chicxulub: Three of a kind? *Annual Review of Earth and Planetary Sciences*, *28*(1), 305–338. https://doi.org/10.1146/annurev.earth.28.1.305

Grieve, R. A. F., Reimold, W. U., Morgan, J., Riller, U., & Pilkington, M. (2008). Observations and interpretations at Vredefort, Sudbury, and Chicxulub: Towards an empirical model of terrestrial impact basin formation. *Meteoritics & Planetary Sciences*, *43*(5), 855–882. https://doi.org/10.1111/J.1945-5100.2008.TB01086.X

Gulick, S. P. S., Barton, P. J., Christeson, G. L., Morgan, J. V., McDonald, M., Mendoza-Cervantes, K., et al. (2008). Importance of pre-impact crustal structure for the asymmetry of the Chicxulub impact crater. *Nature Geoscience*, *1*(2), 131–135. https://doi.org/10.1038/ngeo103

Gulick, S. P. S., Christeson, G. L., Barton, P. J., Grieve, R. A. F., Morgan, J. V., & Urrutia-Fucugauchi, J. (2013). Geophysical characterization of the Chicxulub impact crater. *Reviews of Geophysics*, *51*(1), 31–52. https://doi.org/10.1002/ROG.20007

Hart, R. J., Connell, S. H., Cloete, M., Maré, L., Drury, M., & Tredoux, M. (2000). 'Super magnetic' rocks generated by shock metamorphism from the centre of the Vredefort impact structure, South Africa. *South African Journal of Geology*, *103*(2), 151–155. https://doi.org/10.2113/103.2.151

Hasterok, D., Halpin, J. A., Collins, A. S., Hand, M., Kreemer, C., Gard, M. G., & Glorie, S. (2022). New maps of global geological provinces and tectonic plates. *Earth-Science Reviews*, *231*, 104069. https://doi.org/10.1016/J.EARSCIREV.2022.104069

Hergarten, S., & Kenkmann, T. (2015). The number of impact craters on Earth: Any room for further discoveries? *Earth and Planetary Science Letters*, *425*, 187–192. https://doi.org/10.1016/J.EPSL.2015.06.009

Huber, M. S., Kovaleva, E., Clark, M. D., Riller, U., & Fourie, F. D. (2022). Evidence from the Vredefort Granophyre Dikes points to crustal relaxation following basin-size impact cratering. *Icarus*, *374*, 114812. https://doi.org/10.1016/j.icarus.2021.114812

Huber, M. S., Kovaleva, E., Rae, A. S. P., Tisato, N., & Gulick, S. P. S. (2023). Can Archean impact structures be discovered? A case study from Earth's largest, most deeply eroded impact structure. Additional data [Dataset]. Zenodo. https://doi.org/10.5281/zenodo.7930128

Ivanov, B. A. (2005). Numerical modeling of the largest terrestrial meteorite craters. *Solar System Research*, *39*(5), 381–409. https://doi.org/10.1007/s11208-005-0051-0

Ivanov, B. A., Deniem, D., & Neukum, G. (1997). Implementation of dynamic strength models into 2D hydrocodes: Applications for atmospheric breakup and impact cratering. *International Journal of Impact Engineering*, *20*(1–5), 411–430. https://doi.org/10.1016/S0734-743X(97)87511-2

Kamo, S. L., Reimold, W. U., Krosgh, T. E., & Colliston, W. P. (1996). A 2.023 Ga age for the Vredefort impact event and a first report of shock metamorphosed zircons in pseudotachylitic breccias and Granophyre. *Earth and Planetary Science Letters*, *144*(3–4), 369–387. https://doi.org/10.1016/s0012-821x(96)00180-x

Koeberl, C., Reimold, W. U., & Shirey, S. B. (1996). Re-Os isotope and geochemical study of the Vredefort Granophyre: Clues to the origin of the Vredefort structure, South Africa. *Geology*, *24*(10), 913–916. https://doi.org/10.1130/0091-7613(1996)024<0913:ROIAGS>2.3.CO;2

Kovaleva, E., & Habler, G. (2019). Spatial distribution of zircon with shock microtwins in pseudotachylite-bearing granite gneisses, Vredefort impact structure, South Africa. *Journal of Structural Geology*, *129*, 103890. https://doi.org/10.1016/j.jsg.2019.103890

Kovaleva, E., Zamyatin, D. A., & Habler, G. (2019). Granular zircon from Vredefort granophyre (South Africa) confirms the deep injection model for impact melt in large impact structures. *Geology*, *47*(8), 691–694. https://doi.org/10.1130/G46040.1

Krech, W. W., & Chamberlain, P. G. (1974). New techniques for measuring rock fracture energy. *Society of Petroleum Engineers Journal*, *14*(3), 237–242. https://doi.org/10.2118/4060-PA

Lightfoot, P. C., Morrison, G. G., Bite, A., Farrell, P., & Farrell, K. P. (1997). Geochemical relationships in the Sudbury igneous complex: Origin of the main mass and offset dikes. *Economic Geology*, *92*(1), 289–307. https://doi.org/10.2113/gsecongeo.92.3.289

Macdonald, F. A., Bunting, J. A., & Cina, S. E. (2003). Yarrabubba - A large, deeply eroded impact structure in the Yilgarn Craton, Western Australia. *Earth and Planetary Science Letters*, *213*(3–4), 235–247. https://doi.org/10.1016/S0012-821X(03)00322-4

Martini, J. E. J. (1978). Coesite and stishovite in the Vredefort dome, South Africa. *Nature*, *272*(5655), 715–717. https://doi.org/10.1038/272715a0

Melosh, H. J. (2007). A hydrocode equation of state for SiO_2. *Meteoritics & Planetary Sciences*, *42*(12), 2079–2098. https://doi.org/10.1111/J.1945-5100.2007.TB01009.X

Melosh, H. J., Ryan, E. V., & Asphaug, E. (1992). Dynamic fragmentation in impacts: Hydrocode simulation of laboratory impacts. *Journal of Geophysical Research*, *97*(E9), 14735–14759. https://doi.org/10.1029/92JE01632

Molezzi, M. G., Hein, K. A. A., & Manzi, M. S. D. (2019). Mesoarchaean-Palaeoproterozoic crustal-scale tectonics of the central Witwatersrand basin - Interpretation from 2D seismic data and 3D geological modelling. *Tectonophysics*, *761*, 65–85. https://doi.org/10.1016/j.tecto.2019.04.004

Morgan, J. V., Gulick, S., Mellett, C. L., & Green, S. L. (2017). *Volume 364: Chicxulub: Drilling the K-Pg impact crater* (Vol. 364). International Ocean Discovery Program. https://doi.org/10.14379/iodp.proc.364.2017

Morgan, J. V., Gulick, S. P. S., Bralower, T., Chenot, E., Christeson, G., Claeys, P., et al. (2016). The formation of peak rings in large impact craters. *Science*, *354*(6314), 878–882. https://doi.org/10.1126/SCIENCE.AAH6561

Moser, D. E. (1997). Dating the shock wave and thermal imprint of the giant Vredefort impact, South Africa. *Geology*, *25*(1), 7–10. https://doi.org/10.1130/0091-7613(1997)025<0007:DTSWAT>2.3.CO;2

Moser, D. E., Cupelli, C. L., Barker, I. R., Flowers, R. M., Bowman, J. R., Wooden, J., & Hart, J. R. (2011). New zircon shock phenomena and their use for dating and reconstruction of large impact structures revealed by electron nanobeam (EBSD, CL, EDS) and isotopic U–Pb and (U–Th)/He analysis of the Vredefort domeThis article is one of a series of papers published in this Special Issue on the theme of Geochronology in honour of Tom Krogh. *Canadian Journal of Earth Sciences*, *48*(2), 117–139. https://doi.org/10.1139/E11-011

Pierazzo, E., Vickery, A. M., & Melosh, H. J. (1997). A reevaluation of impact melt production. *Icarus*, *127*(2), 408–423. https://doi.org/10.1006/ICAR.1997.5713

Pilkington, M., & Grieve, R. A. F. (1992). The geophysical signature of terrestrial impact craters. *Reviews of Geophysics*, *30*(2), 161–181. https://doi.org/10.1029/92rg00192

Pirajno, F., & Hoatson, D. M. (2012). A review of Australia's Large Igneous Provinces and associated mineral systems: Implications for mantle dynamics through geological time. *Ore Geology Reviews*, *48*, 2–54. https://doi.org/10.1016/J.OREGEOREV.2012.04.007

Portenga, E. W., & Bierman, P. R. (2011). Understanding Earth's eroding surface with ^{10}Be. *Geological Society of America Today*, *21*(8), 4–10. https://doi.org/10.1130/G111A.1

Rae, A. S. P., Collins, G. S., Morgan, J. V., Salge, T., Christeson, G. L., Leung, J., et al. (2019a). Impact-induced porosity and microfracturing at the Chicxulub impact structure. *Journal of Geophysical Research: Planets*, *124*(7), 1960–1978. https://doi.org/10.1029/2019JE005929

Rae, A. S. P., Collins, G. S., Poelchau, M., Riller, U., Davison, T. M., Grieve, R. A. F., et al. (2019b). Stress-Strain evolution during peak-ring formation: A case study of the Chicxulub impact structure. *Journal of Geophysical Research: Planets*, *124*(2), 396–417. https://doi.org/10.1029/2018JE005821

Reimold, W. U. (1990). The controversial microdeformations in quartz from the Vredefort Structure, South Africa-a discussion. *South African Journal of Geology*, *93*(4), 645–663.

Schmieder, M., & Kring, D. A. (2020). Earth's impact events through geologic time: A list of recommended ages for terrestrial impact structures and deposits. *Astrobiology*, *20*(1), 91–141. https://doi.org/10.1089/ast.2019.2085

Schreyer, W. (1983). Metamorphism and fluid inclusions in the basement of the Vredefort dome, South Africa: Guidelines to the origin of the structure. *Journal of Petrology*, *24*(1), 26–47. https://doi.org/10.1093/petrology/24.1.26

Siegfried, R., & Simmons, G. (1978). Characterization of oriented cracks with differential strain analysis. *Journal of Geophysical Research*, *83*(B3), 1269. https://doi.org/10.1029/JB083iB03p01269

Stanchits, S., Vinciguerra, S., & Dresen, G. (2006). Ultrasonic velocities, Acoustic emission characteristics and crack damage of basalt and granite. *Pure and Applied Geophysics*, *163*(5–6), 975–994. https://doi.org/10.1007/s00024-006-0059-5

Taylor, S. R. (1992). *Solar system evolution: A new perspective*. Cambridge University Press. https://doi.org/10.1017/CBO9781139164368

Therriault, A. M., Reimold, W. U., & Reid, A. M. (1996). Field relations and petrography of the Vredefort granophyre. *South African Journal of Geology*, *99*, 1–21.

Todd, T. P. (1973). *Effect of cracks on elastic properties of low porosity rocks* Doctoral dissertation, Massachusetts Institute of Technology.

Turtle, E. P., Pierazzo, E., & O'Brien, D. P. (2003). Numerical modeling of impact heating and cooling of the Vredefort impact structure. *Meteoritics & Planetary Sciences*, *38*(2), 293–303. https://doi.org/10.1111/j.1945-5100.2003.tb00265.x

Voice, P. J., Kowalewski, M., & Eriksson, K. A. (2011). Quantifying the timing and rate of crustal evolution: Global compilation of radiometrically dated detrital zircon grains. *The Journal of Geology*, *119*(2), 109–126. https://doi.org/10.1086/658295

Webb, S. J., Cawthorn, R. G., Nguuri, T., & James, D. (2004). Gravity modeling of Bushveld complex connectivity supported by Southern African seismic experiment results. *South African Journal of Geology*, *107*(1–2), 207–218. https://doi.org/10.2113/107.1-2.207

Westgate, M., Manzi, M. S. D., James, I., Andreoli, M. A. G., & Durrheim, R. J. (2022). Seismic constraints on the Trompsburg layered igneous intrusion complex in South Africa using two deep reflection seismic profiles. *Frontiers in Earth Science*, *10*, 839995. https://doi.org/10.3389/feart.2022.839995

Wiggins, S. E., Johnson, B. C., Collins, G. S., Jay Melosh, H., & Marchi, S. (2022). Widespread impact-generated porosity in early planetary crusts. *Nature Communications*, *13*(1), 1–6. https://doi.org/10.1038/s41467-022-32445-3

Wünnemann, K., Collins, G. S., & Melosh, H. J. (2006). A strain-based porosity model for use in hydrocode simulations of impacts and implications for transient crater growth in porous targets. *Icarus*, *180*(2), 514–527. https://doi.org/10.1016/J.ICARUS.2005.10.013

Youssof, M., Thybo, H., Artemieva, I. M., & Levander, A. (2013). Moho depth and crustal composition in Southern Africa. *Tectonophysics*, *609*, 267–287. https://doi.org/10.1016/J.TECTO.2013.09.001

References From the Supporting Information

Bass, J. D. (1995). Elasticity of minerals, glasses, and melts. In T. J. Ahrens (Ed.), *Mineral physics & crystallography*. https://doi.org/10.1029/RF002p0045

Hill, R. (1952). The elastic behaviour of a crystalline aggregate. *Proceedings of the Physical Society Section A*, *65*(5), 349–354. https://doi.org/10.1088/0370-1298/65/5/307

Jamshidibadr, M., Collins, A. S., Salomao, G. N., & Costa, M. (2018). U-Pb zircon ages, geochemistry and tectonic setting of felsic and mafic intrusive rocks of Almogholagh complex, NW Iran. *Periodico di Mineralogia*, *87*(1), 21–53. https://doi.org/10.2451/2018PM761

Mavko, G., Mukerji, T., & Dvorkin, J. (2009). In *The rock physics handbook: Tools for seismic analysis of porous media* (2nd ed.). Cambridge University Press.

Reynard, B., Hilairet, N., Balan, E., & Lazzeri, M. (2007). Elasticity of serpentines and extensive serpentinization in subduction zones: Elasticy of serpentines. *Geophysical Research Letters*, *34*(13), L13307. https://doi.org/10.1029/2007GL030176